Laser and Particle Beams (1988), *vol.* 6, *part* 3, *pp.* 471–491
Printed in Northern Ireland

The role of particle beams and electrical currents in the plasma universe†

By ANTHONY L. PERATT
Los Alamos National Laboratory, Los Alamos, New Mexico 87545

(Received 1 October 1987)

Cosmic plasma physics and our concept of the universe is in a state of rapid revision. This change started with *in-situ* measurements of plasmas in Earth's ionosphere, cometary atmospheres, and planetary magnetospheres; the transition of knowledge from laboratory experiments to astrophysical phenomena; discoveries of helical and filamentary plasma structures in the Galaxy and double radio sources; and the particle simulation of plasmas not accessible to *in-situ* measurement. Because of these, Birkeland (field-aligned) currents, double layers, and magnetic-field aligned electric fields are now known to be far more important to the evolution of space plasma, including the acceleration of charged particles to high energies, than previously thought. This paper reviews the observational evidence for a plasma universe threaded by Birkeland currents and particle beams.

1. Introduction and basic model

1.1. *Birkeland currents*

An electromotive force $\int \mathbf{v} \times \mathbf{B} \cdot ds$ giving rise to electrical currents in conducting media is produced wherever a relative perpendicular motion of plasma and magnetic fields exist (Alfvén 1977; Akasofu 1984). An example of this is the (nightside) sunward-directed magnetospheric plasma that cuts the earth's dipole field lines near the equatorial plane, thereby producing a potential supply that drives currents within the auroral circuit. The tendency for charged particles to follow magnetic lines of force and therefore produce field-aligned currents has resulted in the widespread use of the term 'Birkeland currents' in space plasma physics (Dessler 1984). Their discovery in the earth's magnetosphere in 1974 has resulted in a drastic change in our understanding of aurora dynamics, now attributed to the filamentation of Birkeland charged-particle sheets following the earth's dipole magnetic-field lines into vortex current bundles. The importance of Birkeland currents in astrophysical settings has been stressed by Fälthammar (1986).

Laboratory analogs to the magnetospheric Birkeland currents and a tabulation of possible occurances of Birkeland currents in astrophysical plasmas, with dimensions ranging from 10^2 m to nearly 10^{21} m, and currents of 10^5 A to 10^{19} A, have been given (Peratt 1986a).

1.2. *Field aligned electric fields*

Recent literature in the area of magnetospheric physics reflects considerable interest in magnetic-field-aligned electric fields. Such electric fields can have important consequences in cosmic plasma (Fälthammar 1983), including the 'unfreezing' of

† Paper dedicated to Professor Hannes Alfvén on the occasion of his 80th birthday, 30 May 1988.

0263-0364/88/0003–0471$05.00

magnetic fields, the acceleration of electrons to very high energies, and filamentation of the plasma itself.

In magnetized nonhomogeneous astrophysical plasma, a number of mechanisms are present that can generate field-aligned electric fields. These include anomolous resistivity caused by wave–particle interactions, collisionless thermoelectric effects due to energy-dependent wave–particle interactions, magnetic mirror effects involving trapped particles in magnetic-field gradients, and electric double layers due to localized charge separation. While all of the above mechanisms have been studied in the laboratory and simulated by computer, it is the last mechanism that has been found to be remarkably prolific in producing appreciable potential drops in neutral plasma. Moreover, Birkeland currents and double layers appear to be associated phenomena, and both laboratory experiments (Chan & Hershkowitz 1982) and computer simulations (Peratt & Jones 1986) have shown the formation of a series of double layers along current-carrying plasma filaments or beams.

When double layers (or a series of double layers) form in adjacent Birkeland current filaments, field-aligned electric fields are generated, which then serve to accelerate electrons and ions within these regions.

1.3. *The Bennett pinch*

In cosmic plasma the perhaps most important constriction mechanism is the electromagnetic attraction between parallel currents (Alfvén 1981). A manifestation of this mechanism is the pinch effect as studied by Bennett (1934). As discussed (Alfvén 1981), phenomena of this general type also exist on a cosmic scale and lead to a bunching of currents and magnetic fields to filaments. This bunching is usually accompanied by the accumulation of matter, and it may explain the observational fact that cosmic matter exhibits an abundance of filamentary structures (Peratt 1986a).

Consider a fully ionized cylindrical plasma column or charged particle beam of radius r, in an axial electric field E_Z, that produces an axial current density j_Z. Associated with j_Z is an azimuthal magnetic field B_θ. The current flowing across its own magnetic field exerts a $\mathbf{j} \times \mathbf{B}$, radially inward, pinch force. For the case of equilibrium between the compressing electromagnetic force and the sum p of the electron and ion pressures, p_e and p_i, we have

$$\nabla p = \nabla(p_e + p_i) = \mathbf{j} \times \mathbf{B} \tag{1}$$

By employing the Maxwell equation

$$\nabla \times \mathbf{B} = \mu_0 \mathbf{j} \tag{2}$$

equation (1), and the perfect gas law, we arrive at the Bennett relation

$$2Nk(T_e + T_i) = \frac{\mu_0}{4\pi} I^2 \tag{3}$$

where N is the number of electrons per unit length along the beam, T_e and T_i are the electron and ion (perpendicular) temperatures, I is the total beam current, and k is Boltzmann's constant.

2. Filamentary currents and particle beams in the plasma universe

2.1. *Galactic dimensioned Birkeland currents*

As a natural extension of the size hierarchy in cosmic plasmas, the existence of galactic dimensioned Birkeland currents or filaments has been hypothesized (Peratt &

parameter	simulation value
Galactic current, I_z, A	$2{\cdot}15 \times 10^{19}$
Galactic magnetic field, G	$2{\cdot}5 \times 10^{-4}(B_\theta)$
	$2{\cdot}0 \times 10^{-4}(B_{Z0})$
Plasma temperature, keV	2·0–32·0
Plasma density, n_e, cm^{-3}	$1{\cdot}79 \times 10^{-3}$
Electric field strength, E_{Z0}, mV/m	62
Power emitted in synchrotron radiation, W	$1{\cdot}16 \times 10^{37}$
Radiation burst duration, s	$1{\cdot}28 \times 10^{14}$
Age since contraction initiation, s	$5{\cdot}76 \times 10^{14}$
Total energy delivered to source, ergs	$6{\cdot}3 \times 10^{62}$

TABLE 1. Simulation derived parameters for the double radio galaxy cygnus A

Green 1983; Peratt 1986a, 1986b). By extrapolating the size and strength of magnetospheric currents to galaxies, Alfvén (1977) suggests a number of confined current regions that flow through interstellar clouds and assist in their formation. For example, a galactic magnetic field of the order $B_G = 10^{-9}$–10^{-10} T associated with a galactic dimension of 10^{20}–10^{21} m suggests the galactic current be of the order $I_G = 10^{17}$–10^{19} A. (Table 1)

In the galactic dimensioned Birkeland current model, the width of a typical filament may be taken to be 35 kpc ($\sim 10^{21}$ m), separated from neighboring filaments by a similar distance. Since current filaments in laboratory plasmas generally have a width/length ratio in the range 10^{-3} to 10^{-5}, a typical 35 kpc wide filament may have an overall length between 35 Mpc and 3·5 Gpc with an average length of 350 Mpc.

Figure 1 is an electrical equivalent circuit of the metagalaxy (plasma universe) consisting of a large number of filaments with resistance R, inductance L, and sustaining a series of double layers in each of the filaments.

2.2. *The large scale structure of the plasma universe*

Surface currents, delineating plasma regions of different magnetization, temperature, density, and chemical composition give space a cellular structure (Alfvén & Fälthammar 1963). As current-carrying sheet beams collect into filaments, the morphology of the surface currents is filamentary.

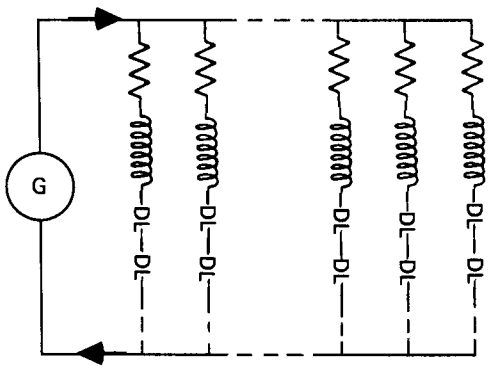

FIGURE 1. Electrical equivalent circuit of the plasma universe. Each filament of plasma is represented by a resistance, inductance, and a series of double layers in which particle beams are accelerated to high energies.

item	The Plasma Universe
Geometry	Euclidean Flat, infinite
Structure	Cellular/Filamentary, all scales
Age	Infinite
Principle molding force	Electromagnetism/Gravitation
Origin of detected radiation	
radio	discrete sources
microwave	discrete sources
optical	discrete sources
X-rays	discrete sources
γ-rays	discrete sources
Origin of the elements	All elements formed in Pre-Metagalactic epoque, continuing synthesis of elements in stars.
Red Shifts	Metagalactic expansion (not more than 90%) matter-antimatter anihilation, plasma convection into filaments, plasma and optical effects.
Quasars, Radio Galaxies	Filamental disruptions (double layers).
Cosmic Rays	Charged particle acceleration in double layers.
'Missing Mass'	Electromagnetic forces.

TABLE 2. Basic properties of the plasma universe

FIGURE 2. Northern Sky map of over one million galaxies brighter than 19th magnitude visible from Lick Observatory. The north galactic pole is at center; the galactic equator is represented by the circle. This map illustrates that the distribution of galaxies on this scale is both cellular and filamentary (adapted from Seldner *et al.* 1977, Ap. J.)

parameter	simulation value
Galactic current, I_z, A	$2{\cdot}15 \times 10^{19}$
Galactic magnetic field, G	$2{\cdot}5 \times 10^{-4}(B_\theta)$
	$2{\cdot}0 \times 10^{-4}(B_{Z0})$
Plasma temperature, keV	2·0–32·0
Plasma density, n_e, cm^{-3}	$1{\cdot}79 \times 10^{-3}$
Electric field strength, E_{Z0}, mV/m	62
Power emitted in synchrotron radiation, W	$1{\cdot}16 \times 10^{37}$
Radiation burst duration, s	$1{\cdot}28 \times 10^{14}$
Age since contraction initiation, s	$5{\cdot}76 \times 10^{14}$
Total energy delivered to source, ergs	$6{\cdot}3 \times 10^{62}$

TABLE 1. Simulation derived parameters for the double radio galaxy cygnus A

Green 1983; Peratt 1986a, 1986b). By extrapolating the size and strength of magnetospheric currents to galaxies, Alfvén (1977) suggests a number of confined current regions that flow through interstellar clouds and assist in their formation. For example, a galactic magnetic field of the order $B_G = 10^{-9}$–10^{-10} T associated with a galactic dimension of 10^{20}–10^{21} m suggests the galactic current be of the order $I_G = 10^{17}$–10^{19} A. (Table 1)

In the galactic dimensioned Birkeland current model, the width of a typical filament may be taken to be 35 kpc ($\sim 10^{21}$ m), separated from neighboring filaments by a similar distance. Since current filaments in laboratory plasmas generally have a width/length ratio in the range 10^{-3} to 10^{-5}, a typical 35 kpc wide filament may have an overall length between 35 Mpc and 3·5 Gpc with an average length of 350 Mpc.

Figure 1 is an electrical equivalent circuit of the metagalaxy (plasma universe) consisting of a large number of filaments with resistance R, inductance L, and sustaining a series of double layers in each of the filaments.

2.2. *The large scale structure of the plasma universe*

Surface currents, delineating plasma regions of different magnetization, temperature, density, and chemical composition give space a cellular structure (Alfvén & Fälthammar 1963). As current-carrying sheet beams collect into filaments, the morphology of the surface currents is filamentary.

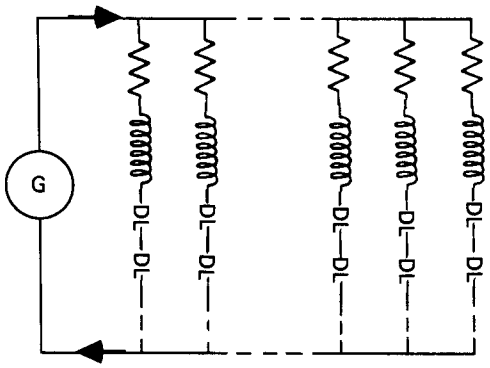

FIGURE 1. Electrical equivalent circuit of the plasma universe. Each filament of plasma is represented by a resistance, inductance, and a series of double layers in which particle beams are accelerated to high energies.

For the case of tenuous cosmic plasmas, the thermokinetic pressure is often negligible and hence the magnetic field is force-free. Under the influence of the electromagnetic fields the charged particles drift with the velocity

$$\mathbf{v} = (\mathbf{E} \times \mathbf{B})/B^2 \tag{4}$$

The overall plasma flow is inwards and matter is accumulated in the filaments which, because of their qualitative field line pattern, are called 'magnetic ropes.' Magnetic ropes should therefore tend to coincide with material filaments that have a higher density than the surroundings. The cosmic magnetic ropes or current filaments are not observable themselves, but the associated filaments of condensed matter can be observed by the radiation they emit and absorb.

It is because of the convection and neutralization of plasma into radiatively cooled current filaments or charged particle beams (due to synchrotron losses) that matter in the plasma universe should often display a filamentary morphology. The Compton thermalization of the synchrotron losses by the active filaments (that contain plasma pinches, stellisimals, and intense particle beams) and the role this process plays in the cosmic microwave background has been investigated by Peter & Peratt (1988).

Table 2 tabulates the basic physical characteristics of the plasma universe while figure 2 shows that the distribution of galaxies at visible wavelengths brighter than 19th magnitude is both cellular and filamentary, as cosmic plasma should be at even greater dimensions.

3. The Biot-Savart force in cosmical electrical networks

3.1. *Long-Range R^{-1} attraction*

Because of the emf-induced current I_z, a galactic filament can be expected to maintain its columnar, filamental form provided the Bennett-pinch condition is satisfied (equation (3)), i.e., that

$$I_Z^2 > 8\pi NkT/\mu_0, \tag{5}$$

where $T = T_e + T_i$.

In addition to confining plasma in filaments radially, the axial current flow produces another important effect; a long-range interactive force on other galactic filaments (Peratt *et al.* 1980; Alfvén 1982; Peratt & Green 1983). Figure 3 illustrates the

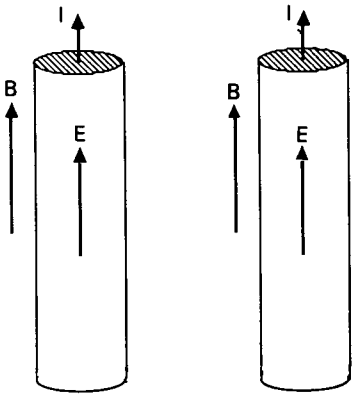

FIGURE 3. Basic geometry under analysis: two parallel Birkeland currents formed by the tendency of charged particles to follow magnetic lines of force **B** and to pinch due to their own induced magnetic field. Because of the magnetic-field-aligned electric field **E**, each filament is a double layer.

geometry under analysis. The Biot-Savart electromagnetic force between filaments is

$$\mathbf{F}_{21} = \int \mathbf{j}_2 \times \mathbf{B}_{21}\, d^3r \tag{6}$$

for all space, where $\mathbf{j} \times \mathbf{B}$ is the Lorentz force. Since the current path greatly exceeds the filament widths, the attractive force between two similarly-oriented filaments is approximately given by

$$F_{21}(I_{Z1}, I_{Z2}) = -\mathbf{r}\frac{\mu_0 I_{Z1} I_{Z2}}{2\pi R} \tag{7}$$

where the subscripts 1 and 2 denote columns 1 and 2, respectively, and R is their separation.

3.2. *Short-range R^{-3} repulsion*

Because of the axial magnetic field B_Z, the particles spiral as they drift or accelerate and thereby produce an azimuthal component in the generalized current $\mathbf{I} = \mathbf{z}I_Z + \theta I_\theta$.

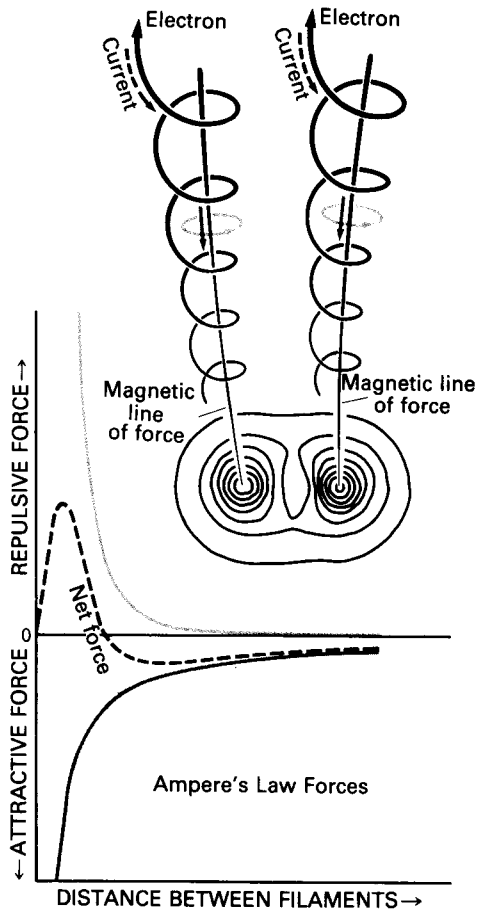

FIGURE 4. The forces between two adjacent Birkeland currents, that is, electric currents aligned along magnetic field lines. The parallel components of current (dark gray lines) are long-range attractive, while the counter-parallel azimuthal currents (light gray rings) are short-range repulsive. A third force, long range electrostatic repulsion, is found if the electrons and ions are not present in equal numbers. These forces cause the currents to form sheets, filaments, or 'magnetic ropes,' and they can be found far from the source region. A projection of the current-induced magnetic fields is shown above the graph.

The force between the azimuthal currents I_θ is

$$\mathbf{F}_{21}(I_{\theta 1}, I_{\theta 2}) = \frac{\mu_0 \pi a}{4\pi R^3} I_{\theta 1} I_{\theta 2} (\mathbf{r} \sin\theta - \boldsymbol{\theta} 2 \cos\theta), \quad R \gg a \tag{8}$$

where $\mathbf{r}$ and θ are the (cylindrical coordinate) unit vectors and a is the radius of an azimuthal current.

Hence, the electromagnetic forces between filaments are ordered as R^{-1} (long-range attractive) and R^{-3} (short-range repulsive). At coalescion distances, the total force is somewhat more complicated than that described by equations (7) and (8). Figure 4 depicts the character of the interaction force as a function of separation distance and a map of B_θ produced by the superposition of induced magnetic fields from each filament.

3.3. *Large scale streaming of filaments*

During long-range attraction, the motion of either filament in the interaction region may be approximately described by the equation $M\,dr^2/dt^2 = \mu_0 I_Z^2 L/4\pi(a-r)$ with a corresponding velocity,

$$v = dr/dt = I_Z(\mu_0 L/2\pi M)^{\frac{1}{2}}(\ln a/a - r)^{\frac{1}{2}} \tag{9}$$

where L is the length of the filamental region involved in Biot–Savart attraction, M is the total mass, $2a$ is the distance of separation between filaments. If the filaments are sufficiently separated so that the logarithmic correction is of order unity, the velocity is approximately given by,

$$v \approx I_Z(\mu_0 L/2\pi M)^{\frac{1}{2}} \quad \{v \approx I_Z(2L/c^2 M)^{\frac{1}{2}} = B_\theta\, d/2\sqrt{2L/M}\}_{cgs}. \tag{10}$$

For a galactic current of $I_Z \sim 2 \times 10^{19}$A, $2a = 2{\cdot}44 \times 10^{21}$ m (~80 kpc), and a mass per unit length of 10^{41} kg/10^{21} m (10^{44} g/35 kpc), the long range attraction between filaments is approximately 1000 km/sec (Peratt & Green 1983; Peratt 1986a). The value of the mass per unit length assumes a plasma mass and length of the order of that observed in galaxies. The salient feature of a plasma universe is that galaxies must form in pinches along (interacting) filaments and these must have velocities of the order of 1000 km/s where currents or fields with the magnitudes and dimensions given above exist.

While early criticisms were directed both at the filamentary or cylindrical nature of the model and the prediction that the interactions would lead to a velocity of 1000 km/s on a large scale (Peratt *et al.* 1980, 1981), recent observations suggest that both filaments of galaxies and their large scale streaming exist.

Collins (1986) report that galaxies at a mean redshift of 5100 km/s, estimated mean distance 100 Mpc, show a systematic streaming velocity of 970 km/s in the direction $l = 305$, $b = 47$ in galactic coordinates. A second group (Burstein *et al.* 1986) simultaneously reported quite similar results.

Tully (1986), analyzing clusters of galaxies demonstrated the existence of a large-scale structure more than 600 Mpc in length, the long axis of this megacluster being aligned toward $l = 300$, $b = 60$. Batuski and Burns (1985) have compiled a map of a 300 Mpc long filament of galaxies. Lerner (1986) discusses the importance of these discoveries to the plasma universe.

4. Synchrotron emission from pinched particle beams

One of the most important processes that limit the energies attainable in particle accelerators is the radiative loss by electrons accelerated by the magnetic field of a

betatron or synchrotron. This mechanism was first brought to the attention of astronomers by Alfvén & Herlofson (1950); a remarkable suggestion at a time when plasma, magnetic fields, and laboratory physics were thought to have little, if anything, to do with a cosmos filled with 'island' universes (galaxies).

Synchrotron radiation is characterized by a generation of frequencies appreciably higher than the cyclotron frequency of the electrons; a continuous spectra (for a population of electrons) whose intensity decreases with frequency beyond a critical frequency (near intensity maxima); increasing beam directivity with increasing γ ($\gamma = (1-\beta^2)^{-\frac{1}{2}}$); and strongly polarized electromagnetic wave vectors.

4.1. *Synchrotron emitting Z-pinches*

Charged particle beams held together or pinched by their self magnetic fields have been of general interest since their earliest investigation by Bennett (1934). The macroscopic picture of such a beam is that of a self-consistent magnetic confinement or compression against the expansion due to thermal pressure [equation (5)]. On the microscopic scale, the individual particles orbits include radial oscillations due to the Lorentz force superimposed on the drift in the direction of mean flow. These are the betatron oscillations. Since they imply particle acceleration, there is electromagnetic radiation associated with them. Because the force is a $\mathbf{v}\times\mathbf{B}$ force, the radiation from the relativistic electrons is synchrotron radiation.

Manifestations of the pinch effect appear for a laboratory observer as a rapidly occurring phenomena. A burst of radiation from high-current discharges (with current densities of the order 10^{11} A/cm^2), such as low-inductance vacuum sparks, plasma focus devices, and exploded wires is found over a broad spectral range; from the microwave region to the hard X-ray region. Recorded data show that the radiation bursts are correlated with dips in the current waveform. Analysis of the directional patterns of the millimeter radiation shows that the microwave radiation is synchrotron radiation of electrons in the magnetic field of the proper current. The hard X-ray quanta are attributed to synchrotron radiation from the electrons at the transitions between Landau levels in this same current-induced magnetic field (Meierovich 1984).

The total synchrotron power radiated incoherently from a Maxwellian distribution of electron velocities, over all frequencies, is given by (Bekefi 1966)

$$p_{\text{syn}} = \left\{\frac{4e^4}{3m_e^2c^3} B^2 n_e \beta_Z^2\right\}_{cgs} \text{ ergs/cm}^3. \tag{11}$$

Similar expressions applicable for the determination of the average power radiated per unit length for relativistic Bennett pinches have been given by Meierovich (1984) and Newberger *et al.* (1984).

4.2. *Synchrotron bursts*

An enhancement of radiated power, given by equation (11), is achieved when the sum of the $\mathbf{v}\times\mathbf{B}$ radial forces seen by the relativistic electrons [equation (6)] is increased, as is the case when the azimuthal magnetic fields of neighboring pinches are present (figure 4). While no theoretical treatment of synchrotron enhancement from beam interactions is known, this phenomena has been examined in some detail, both experimentally and with simulations. Whenever the attractive force between simulation columns causes their separation to be reduced to a distance such that the repulsive force equation (8) starts to become comparable to the attractive force equation (7), a burst in the radiation occurs [figure 5]. For the parameters used in these simulations,

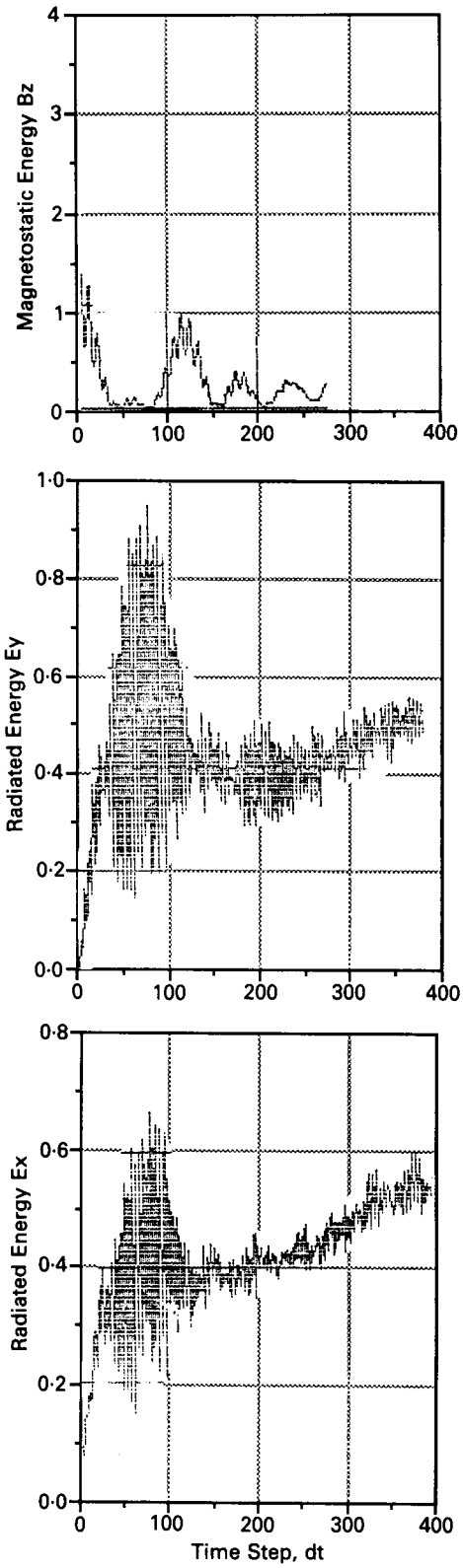

FIGURE 5. (a) Self-consistent axially-directed magnetic field energy versus time. (b) and (c) Energy lost via synchrotron radiation in the x and y electric field components, respectively. The ordinate is in arbitrary energy units of $7{\cdot}1 \times 10^5$ j while the abscissa is in simulation time units $dt' = 6 \times 10^{11}$ s. T is the time in dt' time steps.

this distance is of the order of several pinch radii. As shown in figure 5, the radiation from the kiloelectronvolt particles is polarized in the transverse plane and the synchrotron enhancement (burst) is detected in the **x** and **y** electric radiation energies (W_{ERx}, W_{ERy}) and the **z** magnetic radiation energy (W_{BRz}). The burst lasts until the induced axial magnetostatic energy W_{Bz}, due to the azimuthal current, I_θ, is depleted (because the counterparallel azimuthal current force equation (8) brakes the azimuthal electron flow in both filaments). For some simulational parameters, W_{Bz} can build-up and discharge again in the form of additional bursts of synchrotron radiation. The long-time, slowly-varying increase in radiation in W_{ERx} and W_{ERy} is due to the buildup of electrostatic energy from charge separation in the particle number and size constrained simulation model. The cell size and time step parameters used in the simulations are $\Delta' = 1{\cdot}66 \times 10^{20}$ m and $dt' = 5{\cdot}87 \times 10^{11}$ s.

4.3. *Double radio sources*

The existence of double radio galaxies presents a major challenge to cosmological theories. Cygnus A, the brightest radio source in the constellation Cygnus, has proved to be the 'prototype' of double radio galaxies and models of double galaxies are usually based on the characteristics of this source. Many excellent reviews on the properties of double radio sources observed from the 1960's on are available in the literature (e.g., Miley 1980, Perola 1981), as are a number of models of sources. However, regardless of whatever ingredients are postulated as necesary in models used to 'explain' their existence, what is observed from any radio source is *synchrotron radiation,* which requires only the presence of relativistic electrons in a magnetic field.†

Any plausible theory on double radio galaxies should be expected to explain the following:

(1) The origin and source of energy of double radio galaxies.
(2) The total magnitude of the radio flux observed.
(3) The measured flux density as a function of frequency.
(4) The observed isophotal morphologies.
(5) The spatially varying power law within a source.
(6) The polarization properties of the incoherent synchrotron radiation measured.
(7) The lifetime and evolution of a source.

Additionally, in item 4, it is also necessary to explain the radiation 'hot spots' in classical radio doubles; their diametric displacement off an imaginary axis running from giant radio lobe to giant radio lobe through an elliptically shaped center; the relationship between "bridges" and so-called "jets" connecting the elliptical center with the lobes; the one-sidedness of jets in quasars and powerful sources; multi-knotted features in hot spots, bridges, and jets; the apparent superluminosity of some sources; and the problem of a nearly uniformly fading of some jets, thousands of light years in extent, in a few decades.

4.4. *Power emitted from double radio sources*

An estimate of the total power emitted as synchrotron radiation follows directly from the simulations. During the radiation 'burst era' at $T = 90$, the total energy radiated in the form of electric and magnetic field energy is $W_{\text{rad}} = 2{\cdot}1$ AEU (arbitrary energy units) while the total simulation magnetostatic energy is $W_{ms} = 350$ AEU. Since, at

† Alfvén (1986a, b), Bostick (1986), and Lerner (1985a, b; 1986) have proposed similar plasma radio source models also based on the delivery of energy to the radiation regions via circuit models.

$T = 90$, $B_Z = 2{\cdot}0 \times 10^{-8}$ T, $B_\theta = 2{\cdot}5 \times 10^{-8}$ T, and $V \sim 10^{63}$ m^3 is the plasma volume; $W_{ms} = (2\mu_0)^{-1} B^2 V = 2{\cdot}5 \times 10^{53}$ J, or 1 AEU $= 7{\cdot}1 \times 10^{50}$ J. The peak radiation burst lasts $\sim 20dt'$ in the compressed time frame (figure 5), corresponding to an actual time of $20(6 \times 10^{11}\text{ s})\sqrt{(1836/16)} = 1{\cdot}28 \times 10^{14}$ s. The total power emitted in synchrotron radiation is $L = 2{\cdot}1 \times 7{\cdot}1 \times 10^{50}\text{ J}/1{\cdot}28 \times 10^{14}\text{ s} = 1{\cdot}16 \times 10^{37}$ W, which is to be compared with the radio luminosity of Cyg A of $1{\cdot}6$–$4{\cdot}4 \times 10^{37}$ W.

The synchrotron power derived above is also available from equation (11). At $T = 90$, the velocity distribution of the Birkeland electrons is nearly Maxwellian with a mean energy of 26·49 KeV, or $\beta_Z = 0{\cdot}228$. From equation (11), $P_{syn} \approx 3{\cdot}17 \times 10^{-15} B^2 n_e \beta^2 = 2{\cdot}06 \times 10^{-33}$ W/cm^2. The total power or luminosity is then $L = P_{syn} V = 2{\cdot}06 \times 10^{36}$ W, i.e., about a factor of 6 less than $1{\cdot}16 \times 10^{37}$ W resulting from the filament interaction (c.f., figure 5).

4.5. *Isophotal patterns of double radio sources*

Improvements in measurements of synchrotron radiation from double radio galaxies and 3D EM simulations share many simularities. Figure 6a shows one of the first low resolution intensity maps of the double source Fornax A. Its low resolution

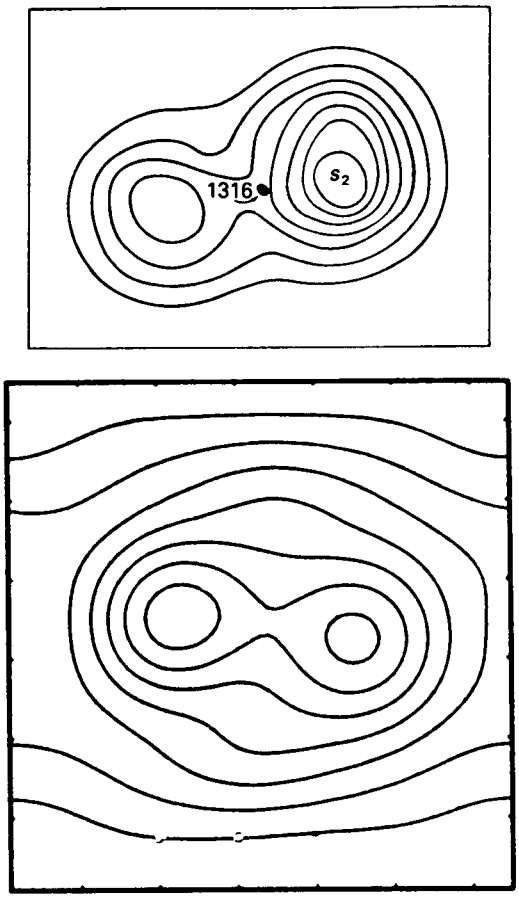

FIGURE 6. (a) Low resolution intensity contours of the double radio source Fornax A. The peculiar galaxy NGC 1316 is shown between the radio lobes. (b) Low resolution magnetic isobars of interacting Birkeland currents during synchrotron burst era.

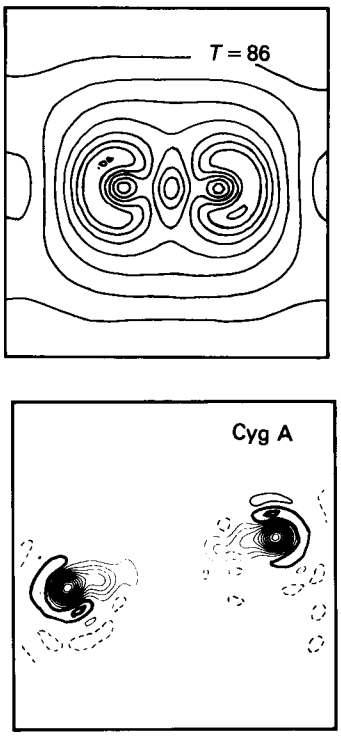

FIGURE 7. (a) Isophotal contours of synchrotron radiation at 150 MHz from Cyngus A. (b) Magnetic energy isophotes of filament cross sections near synchrotron burst peak $T = 86$ (17·5 Myr).

counterpart, discovered while investigating the morphology of z-pinches during synchrotron burst is shown in figure 6b.

At higher resolution, 'hot spots,' diametrically positioned in the two lobes, are observable (figure 7). With yet better resolution, fine detail structure in the self-consistent magnetic energy density and in the induced electric energy density, responsible for supplying energy to the synchrotron radiating electrons, are mapable. The simulations allow a frame-by-frame analysis of a synchrotron source as it develops in time. The simulations also show that both the 'remarkable' alignment of lobes and hot spots and energy output, often attributed to a dense object located between lobes, is due to the transport of energy within two interacting current-carrying filaments. The filaments act as transmission lines and transport energy, a portion of which is lost in synchrotron radiation. The transmission lines are not observable in the visible, however, the plasma compressed by the magnetic isobaric sump between filaments can radiate in the visible (Peratt 1986a). The release of large amounts of energy in small volume discharge regions has resulted in astrophysical hypotheses that the energy *source* in these regions is due to exotic, high-mass objects.

The approximate age of a double radio galaxy can be determined from its isophotal contour profile at a given wavelength; the isophotes of strong classical double (early) radio galaxies are largely determined by the magnetic energy density of the interacting Birkeland filaments, while (later time) double radio galaxies project more complicated patterns resulting from the induction acceleration of plasma confined between the magnetic isobars. Figure 8 illustrates this situation by comparing the synchrotron

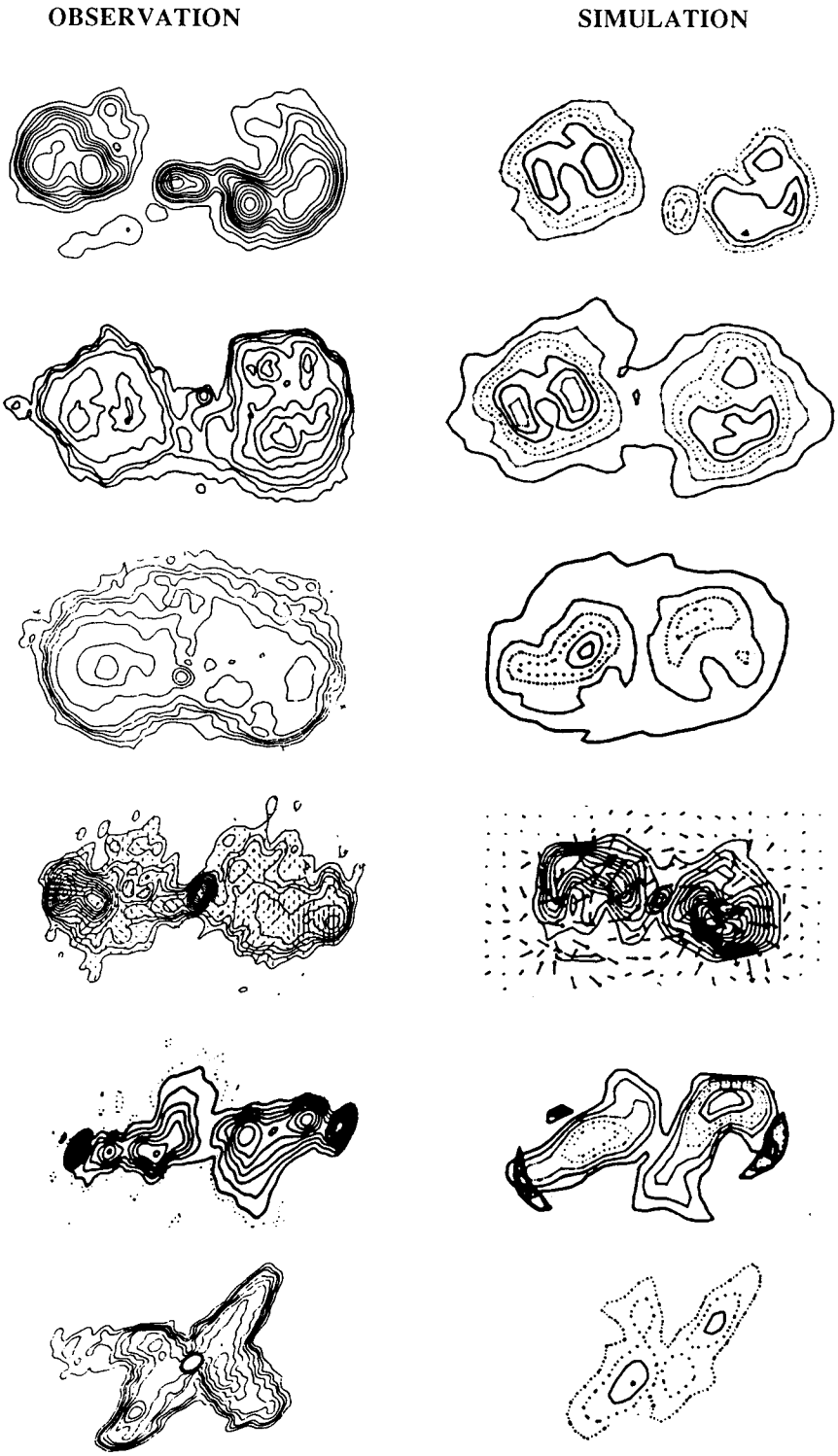

FIGURE 8. (left column) Synchrotron isophotes (various frequencies) of the double radio sources 0844 + 319, Fornax A, 3C310, 2355 + 490, 3C192, and 3C315. (right column) Simulation analogs (Run T06) at times $T = 51$, 52, 236 (reverse), 237, 280, and 288 (reverse).

isophotes to the induction electric field energy patterns for several sources, extragalactic and simulation.

Frame-by-frame, the hot-spot 'cusps' move inward with time, the 'central component' becomes a hotter and a more intense radiator, while the radiation isophotes take on a 'butterfly' like pattern that finally extinguishes as the synchrotron burst era comes to an end in the embryo stage of the development of a galaxy.

5. The formation and evolution of galaxies in cosmic plasma

The evolution of cosmic plasma from a filamentary state to the development of double radio sources and quasars, then a variety of galaxy morphological types, using fully three-dimensional, fully electromagnetic, particle-in-cell simulations was previously reported (Peratt 1986a, 1986b). The importance of electromagnetic forces in galactic and stellar evolution derives from the fact that the universe is largely matter in its plasma state. The observed stars are composed of plasmas, as are the interstellar

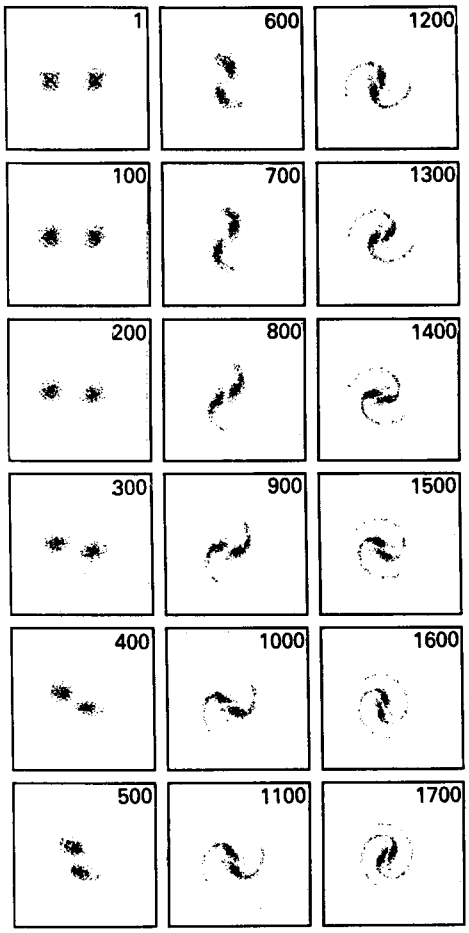

FIGURE 9. Single frame stills of plasma in galaxy simulation run DD4: $\omega_c/\omega_p = 3.0$, $T_{e0} = T_{i0} =$ 32 keV, $T = 1$–1700. Acceleration field, 62 mV/m. Not shown is the intergalactic plasma trapped in the elliptical sump at the geometric center of the simulation. This plasma tends to obscure the coalescion region.

and interplanetary media and the outer atmospheres of planets. The neutral HI regions in galaxies are also plasma although the degree of ionization is probably only 10^{-4}. Both the intra and intergalactic medium then consists of plasma, leading to the coinage of the term 'plasma universe'. Electromagnetic forces, that are 39 orders of magnitude stronger than the gravitational force, can then be expected to play a crucial role in the development of the plasma universe including both the formation of systems of galaxies and the formation of stars within the dusty galactic plasmas.

The evolutionary sequence of interacting plasma filaments is shown in figure 9. Depicted in this figure are the cross sections of the filaments where field-aligned electric fields are present. The morphologies and radiation properties of the simulated plasmas shown in figure 9 suggest a transition through the following sequence of cosmic objects: double radio galaxy to radioquasar; radioquasar to radio quiet QSO's (quasi-stellar objects); radio quiet QSO's to peculiar and Seyfert spiral galaxies; and peculiar and Seyfert galaxies to normal and barred galaxies.

5.1. *The barred spiral galaxy NGC 1300*

The spiral galaxy NGC 1300 (figure 10a) is perhaps the most perfect example of a barred spiral. Classified as type SBb, NGC 1300 has a visual magnitude of 11·3, an apparent size of $6{\cdot}0' \times 3{\cdot}2'$, and is thought to be located at a distance of 13·8 Mpc.

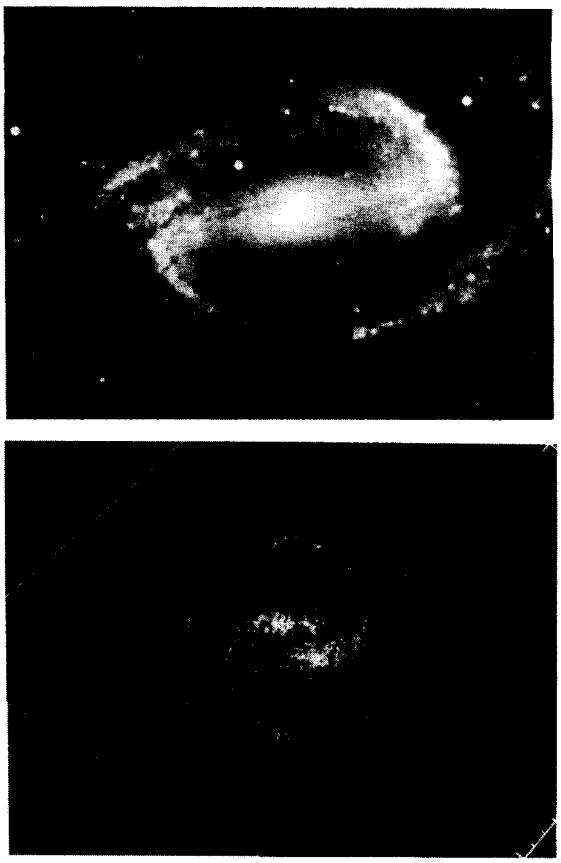

FIGURE 10. (a) Optical photograph of the SBb galaxy NGC 1300. (b) Single frame still of simulated galaxy plasma (Run DD4) at time $T = 1750$.

The plasma analog of NGC 1300, unexpectedly discovered while investigating the long term evolution of plasma in galactic-dimensioned Birkeland filaments, is shown in figure 10b. Delineating features are apparent in both NGC 1300 and its analog.

In bulk morphology both are two-armed spirals that can be judged as belonging to type SBb. Striations are observable in the arms of both, whose patterns closely resemble Baade's classic description of matter in spiral arms appearing like 'beads on a string.' Both also display a band across the bar that extends to the juncture of each arm, then bends with the arm. This band also allows the identification of an inner and an outer portion of a spiral arm. Differences in NGC 1300 and its analog include the obscuration of the nucleus, not seen in the simulation as the elliptical core formed at early time (Peratt 1986b) is not included in the particular simulation depicted in figure 10. Additionally, the simulated galaxy represents a younger stage in the development of a SBb galaxy. The plasma flowing through the central bar is just beginning to form the inner arm along the trailing outer arm. This structure is already well-formed in NGC 1300. It is of interest to note that the (inner arm) plasma flowing 'outward' from the central bar region, as-well-as the 'outward' flowing or trailing outer arm agree with Arp's hypothesis regarding the ejection of spiral arms from the core.

5.2. *Rotational velocities of spiral galaxies*

Figure 11 shows the radial velocity versus distance from the galaxy center typical of spiral galaxies. The data show (i) a nearly linear, solid body rotation for the galaxy center (the first few arcminutes from center), (ii) a nearly radially independent velocity profile in the spiral arms, and (iii) distinct structure in the spiral arms that appears on

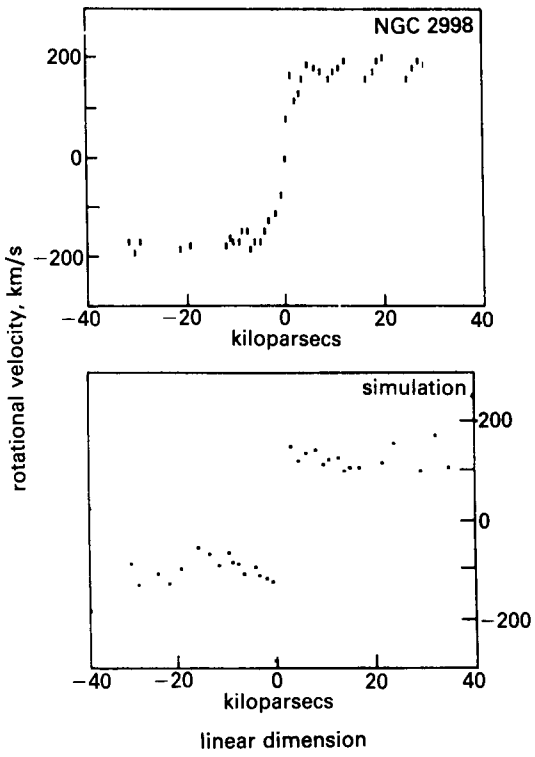

FIGURE 11. Spiral galaxy rotational velocity characteristics. (a) NGC 2998. (b) Simulation, run DD4, $T = 1750$.

the so-called 'flat' portion of the velocity curve (beyond the first few arcminutes or, equivalently, the first few kiloparsecs from the center of the galaxy).

The simulated velocity curve in figure 11 corresponds to the spiral galaxy in figure 9 at time $T = 1750$ (this curve is the differential rotation measured between $T = 1749$ and 1750). The simulation data illustrate that (i) the plasma core rotates very nearly as a solid body, and (ii) the spirals arms grow in length as they trail out along the magnetic isobars. The arms do not wind up around the core because the magnetic field gradient increases inward. Concomittant with the lengthening of the arms is a thining of the arms. Because of this, and the axial current conducted through the thin plasma arms, a diocotron instability is produced. The effect of this instability shows up in both the cross-sectional views of the spirals arms (figure 9, late time) and in the velocity profile (figure 11). Because the plasma in the spiral arms is very nearly neutral (the $\mathbf{B} \times \nabla B$ charge separation prevents completely local neutrality) the diocotron instability is moderated somewhat. The azimuthal (sideways) velocity of this instability is given by $V = V' \cot(\psi)$, where V' is the slowly varying radial velocity component and $\psi = \psi(n_e, \mathbf{B}, v_e)$, where v_e is the effective electron collision frequency in the arm. Good examples of this are found in the Sc type galaxies. For example, M101, NGC 253, NGC 2998 and NGC 3646. (Peratt 1986b) and NGC 3495, NGC 753, NGC 801, and NGC 2885 (Arp 1986).

One consequence of the plasma model for spiral galaxies is a reinterpretation of the Tully–Fisher relation that relates rotation velocity to the brightness of stellar populations. Both rotation velocity and star formation (Section 5.3) are functions of current I. Where I is strong, spiral galaxies rotate rapidly. Additionally, the stronger current also enhances the production of bright stars in the plasmas pinched in the arms of spiral galaxies.

5.3. *Pinching of filaments to the condense state*

The importance of the pinch effect in interstellar plasma clouds located in galactic dimensioned, current-conducting plasma is illustrated by the following two examples:

1. Consider first an interstellar cloud of 100 solar masses, $M_c = 2 \times 10^{32}$ kg, occupying a volume of the linear dimension $l_c = 10^{17}$ m. The temperature of the cloud is $T_c = 10$–10^2 K. This represents a cloud of approximately the same mass as the Orion nebula. The number of atoms present in the cloud is $\sim 10^{59}$, implying a mean density of $n = 10^8\ \mathrm{m}^{-3}(10^2\ \mathrm{cm}^{-3})$ and giving $N = 10^{42}$ atoms m^{-1}. Putting the latter figure and the temperature above into the Bennett relation equation 3, we find that an electric current of $I_c \sim 5 \times 10^{13} - 2 \times 10^{14}$ A has to flow through the cloud in order to produce a considerable compressional effect.

2. Consider next a cloud of one solar mass only, $M_c = 2 \times 10^{30}$ kg, having a temperature of $T_c = 10$–10^2 K and an extent of $l_c = 10^{16}$–10^{17} m. Hence $n = 10^6$–$10^9\ \mathrm{m}^{-3}$ (1–$10^3\ \mathrm{cm}^{-3}$) and $N = 10^{40}$–10^{41} atoms m^{-1}. The current needed to compress the cloud is now found to be $I_c = 5 \times 10^{12}$–5×10^{13} A.

The current density for both cases outlined above is approximately $0{\cdot}1$–$1{\cdot}0 \times 10^{-20}\ \mathrm{A/m^2}$. For the simulated spiral galaxy, $l_c \sim 10$ kpc, $I \sim 10^{20}$ A, so that $j \sim 0{\cdot}1 \times 10^{-20}\ \mathrm{A/m^2}$ and the threshold for star formation is met. [Star formation in the elliptical sump is expected to start much earlier than in the spiral arms because of the compressive forces on the dense plasma contained there].

In the analytical examples above the interstellar clouds were assumed to be contracted by a Bennett pinch, implying a pure toroidal magnetic field and a pure axial current. According to Alfvén & Carlqvist (1978), all magnetic configurations ranging

from this kind of pinch to the force-free states would also give rise to contractive forces. For the plasma to pinch in these cases the total current must be larger than that given by the Bennett relation. For the total current I_Z conducted by the galaxy to reach the threshold current density for star formation, it is required that the double layer electric field E_Z exist at least to times comparable with the time to spiral formation, i.e., $T \sim 1000$ or 2×10^8 years.

5.4. *The formation of stars*

Theories concerning the origin of the Sun and other stars clearly also must have a foundation in hydromagnetics and plasma physics (Alfvén & Arrhenius 1976). From this study they conclude that the primeval Sun, surrounded by plasma from which it condensed, had a mass approximately the same as today but a radius of the order of 10^{12} cm (out to Pluto). Its spin and magnetization were also much larger. Based on the Brownlee–Cox model (1961), the radius of the Sun would have remained at about 10^{12} cm during a deuterium burning stage. This stage would last about 10^8 yr before contraction to its present hydrogen-burning stage.

It is therefore of interest to compare the total simulation time and its sequence of evolutionary plasma products, double radio galaxies to barred spiral galaxies, to astronomical estimates of the ages of galaxies and the ages of stars, or star clusters, formed in galaxies.

Figure 12 is a color–color array with $U-B$ color index (ultraviolet minus blue magnitudes) plotted against the standard color index, $B-V$ (blue minus visual). The main sequence shown in figure 12 is used only as a reference, since stellar plasmas in the main sequence represent the long-term hydrogen burning phase of stars rather than the pinch collapse and contraction phases discussed above. The hydrogen-burning phase may range between 10^6 yr to tens of gigayears while the contraction may range from 10^3 yr to hundreds of megayears for stars whose masses vary from 50 solar masses to 0·1 solar mass ($B-V = -0{\cdot}3$ to $1{\cdot}0$).

Figure 12 shows that the color index, or color, varies from blue to slightly red for the nucleii of QSO's, slightly bluish for galaxy types Irr and Sm, while at type Sd, yellowish

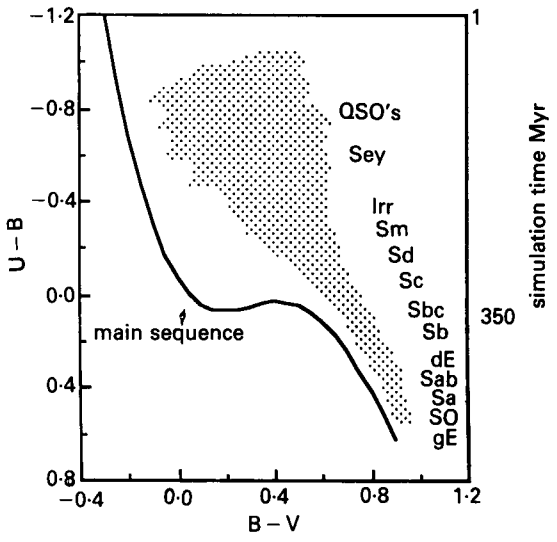

FIGURE 12. Color–Color diagram of galaxy types, $U-B$ (ultraviolet minus blue) vs. $B-V$ (blue minus visible).

at types Sc and Sb, to red for Sa and giant elliptical galaxies. Also plotted on figure 12 is the total simulation time shown in figure 9, $1750\,dt' = 350$ Myr. The time scale has been fitted to the color index $U - B$ so that simulated QSO and SBb phases coincide with their observed counterparts in the sequence of galaxies. The time 1 Myr on this scale represents the time at which the simulation is started, when the Birkeland filaments are well-defined. Plasma in the elliptical sump derives from an era preceding a well-defined pinch and may already be tens or hundreds of megayears old.

Figure 13 is a Hertzsprung–Russel diagram of galactic clusters from which stellar ages are thought inferable (Menzel, Whipple & de Vaucouleurs 1970). The ages of the clusters corresponding to the positions of the breaks from the main sequence are shown by the scale on the right. Since the contraction phase is expected to be much shorter than the hydrogen burning phase, a time indicated on this scale may be the total elapsed time since a cluster formed out of interstellar plasma. Nevertheless, many of the clusters are very young on a cosmic time scale, often less than 10^8 years. For the very young clusters, only the most massive stars have had time to condense and reach the main sequence. The remainder have not yet settled on the main sequence and form a scattered band to the right of it.

An elapsed simulation time of 350 Myr is sufficient for the pinch collapse and contraction of stars from plasma clouds of 0·1 to 50 solar masses, if the simulation had enough particles and cells to resolve this phenomena. This then sets the direction and goals for future particle-in-cell simulations whose intent is to study galactic evolution on yet more powerful computers.

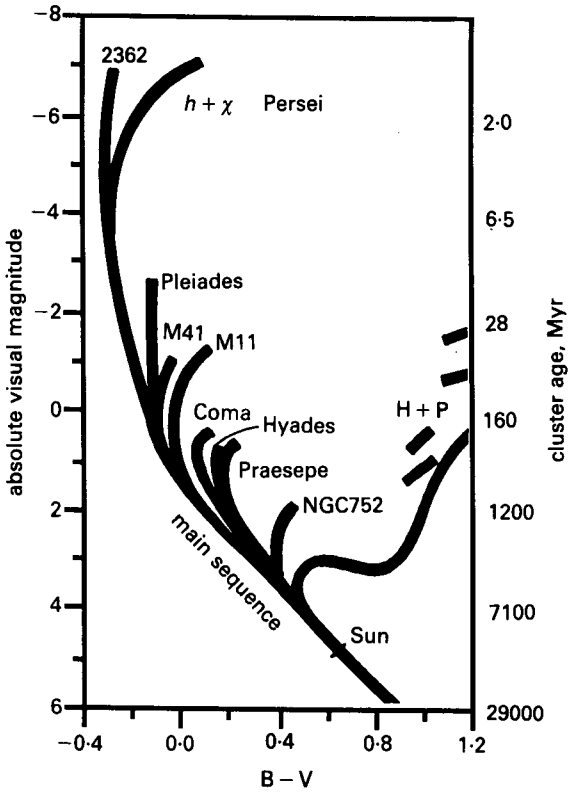

FIGURE 13. Visible magnitude-Color diagram of stars in galactic clusters. The ages of the clusters corresponding to positions of the breaks from the main sequence are shown by the scale on the right. Blue stars (surface temperature 3 keV) are on the left of the diagram while red stars (surface temperature 0·4 keV) are on the right.

The inclusion of stars on the main sequence is expected to account for the morphology of Sa and SBa type galaxies, where the increasing role of gravitation makes its presence felt in the dynamics of late time galaxies (Lerner 1986). Attempts to bridge the fully electromagnetic plasma model consisting of plasma clouds (each simulation particle) to include the gravitational forces between particles representing stellar clusters is currently underway (Peratt 1986b).

6. Conclusions

Because of *in-situ* measurements of plasmas in Earth's ionosphere, cometary plasmas, and the planetary magnetospheres, and recent discoveries of helical and filamentary plasma structures in our Galaxy and in extragalactic radio sources, our understanding of cosmic plasma has changed considerably during the last decade. In particular, Birkeland currents, double layers, and magnetic field-aligned electric fields are now known to play a far more important role in the evolution of plasma in space, including the acceleration of charged particles to high energies. Because the properties of the plasmas in space are found to differ little from those in the laboratory, the empirical knowledge gained from earth-bound experiments has suddenly found application in situations orders of magnitude greater in dimension. Kirchoff's laws for currents in circuits appear equally valid regardless of whether the plasma has its dimensions measured in centimeters, kilometers, parsecs, kiloparsecs, or megaparsecs.

With the advent of three-dimensional electromagnetic particle-in-cell simulations, investigations of Birkeland currents and double layers have become possible in plasmas not accessible to in-situ measurement, i.e., in plasmas having the dimensions of galaxies or systems of galaxies. The necessity for a three-dimensional electromagnetic approach derives from the fact that the evolution of magnetized plasmas involves complex geometries, intense self-fields, nonlinearities, and explicit time dependence. Moreover, synchrotron radiation and double layers are discrete particle phenomena and cannot be studied using magnetofluid models of plasma. The importance of applying electromagnetism and plasma physics to the problem of radio galaxy, galaxy and star formation derives from the fact that the universe is largely matter in its plasma state, i.e., a *plasma universe.* The motion of this plasma in local regions can lead to pinches and ultimately condense states of matter. Where double layers form, strong electric fields can accelerate particles to high energies. These processes are found to form a common link in the evolution of cosmic plasma, from the formation of quasars and double radio galaxies to the condensation of stars in galactic plasmas.

Acknowledgement

This work was supported by the U.S. Department of Energy.

REFERENCES

Alfvén, H. & Herlofson, N. 1950 *Phys. Rev.* **78,** 616.

Alfvén, H. & Arrhenius, G. 1976 *Evolution of the Solar System,* NASA SP-345, Washington, D.C., Chap. 25.

Alfvén, H. 1977 *Rev. Geophys & Space Sci.* **15,** 271.

Alfvén, H. and Carlqvist, P. 1978 *Astrophys. Space Sci.* **55,** 484.

Alfvén, H. 1981 *Cosmic Plasma,* D. Reidel Publ. Co. Dordrecht, Holland.

Alfvén, H. 1982 *Physica Scripta* **T2/1,** 10.

Alfvén, H. 1986a *IEEE Trans. on Plasma Sci.* **PS-14,** 629.

ALFVÉN, H. 1986b *IEEE Trans on Plasma Sci.* **PS-14,** 779.

ALFVÉN, H. and FÄLTHAMMAR, C.-G. 1963 *Cosmical Electrodynamics,* Oxford, Clarendon Press.

AKASOFU, S.-I. 1984 in *Magnetospheric Currents,* T. A. Potemra, Ed. (Geophysical Monograph No. 28), American Geophys. Union, Washington, D.C., 29.

ARP, H. 1986 *IEEE Trans. on Plasma Sci.* **PS-14.**

BATUSKI, D. J. & BURNS, J. O. 1985 *Ap. J.* **299,** 5.

BEKEFI, G. 1966 *Radiation Processes in Plasmas,* John Wiley & Sons, New York, Chap. 6.

BENNETT, W. H. 1934 *Phys. Rev.* **45,** 890.

BOSTICK, W. H. 1986 *IEEE Trans. on Plasma Sci.* **PS-14,** 703.

BROWNLEE, R. R. & COX, A. N. 1961 *Sky and Tel.* **21,** 252.

BURSTEIN, D. *et al.* 1986 in Proc. NATO Workshop (Kona, Hawaii), in press.

CHAN, C. & HERSHKOWITZ, N. 1982 *Phys. Fluids* **25,** 2135.

COLLINS, C. A. 1986 *Nature* **320,** 506.

DESSLER, A. J. 1984 in *Magnetospheric Currents,* T. A. Potemra, Ed. (Geophysical Monograph No. 28), American Geophys. Union, Washington, D.C.

FÄLTHAMMAR, C.-G. 1983 ESA J. **7,** 385.

FÄLTHAMMAR, C.-G. 1986 *IEEE Trans. on Plasma Sci.* **PS-14,** 616.

LERNER, E. J. 1985a *Laser and Particle Beams,* **4,** 193.

LERNER, E. J. 1985b *Laser and Particle Beams* **4,** 223.

LERNER, E. J. 1986 *IEEE Trans. on Plasma Sci.* **PS-14,** 690.

MEIEROVICH, B. E. 1984 *Phys. Reports* **104,** 259.

MENZEL, D. H., WHIPPLE, F. L., & DEVAUCOULEURS 1970 *Survey of the Universe* Prentice-Hall, New Jersey.

MILEY, G. 1980 *Ann. Rev. Astron. Astrophys.* **18,** 165.

NEWBERGER, B. S. *et al.* 1984 *Bull. Am. Phys. Soc.* **29,** 1435.

PERATT, A. L., GREEN, J. & NIELSEN, D. 1980 *Phys. Rev. Letters* **44,** 1767.

PERATT, A. L., & GREEN, J. C. 1981 *IEEE Conference Record, Santa Fe, New Mexico, p.* 64.

PERATT, A. L. & GREEN, J. C. 1983 *Astrophys. Space Sci.* **91,** 19.

PERATT, A. L. 1986a *IEEE Trans. on Plasma Sci.* **PS-14,** 639.

PERATT, A. L. 1986b *IEEE Trans. on Plasma Sci.* **PS-14,** 763.

PERATT, A. L. & JONES, M. E. 1986 *IEEE Conf. Record,* Saskatoon, Canada.

PEROLA, G. C. 1981 *Fund. Cosmic Phys.* **7,** 59.

PETER, W. and PERATT, A. L. 1988 *Laser and Particle Beams* (this issue).

TULLY, R. B. 1986 *Astrophys. J.* **303,** 25.